JACS
JOURNAL OF THE AMERICAN CHEMICAL SOCIETY
Article
pubs.acs.org/JACS

Switching the Enantioselectivity in Catalytic [4 + 1] Cycloadditions by Changing the Metal Center: Principles of Inverting the Stereochemical Preference of an Asymmetric Catalysis Revealed by DFT Calculations

Shivnath Mazumder,[†] Douglas W. Crandell,[†] Richard L. Lord,[‡] and Mu-Hyun Baik*[,†,§]

[†]Department of Chemistry, Indiana University, 800 E. Kirkwood Avenue, Bloomington, Indiana 47405, United States
[‡]Department of Chemistry, Grand Valley State University, 1 Campus Drive, Allendale, Michigan 49401, United States
[§]Department of Materials Chemistry, Korea University, Jochiwon-eup, Sejong-si, 339-700, South Korea

Supporting Information

ABSTRACT: The mechanisms of the asymmetric [4 + 1] carbocyclization of vinylallenes with carbon monoxide catalyzed by Pt(0) and Rh(I) carrying the chiral support ligand (*R*,*R*)-Me-DuPHOS (Me-DuPHOS = 1,2-bis(2,5-dimethylphosphorano)benzene) were studied using density functional theoretical models. Previously, it was observed that the (*R*)-stereoisomer of the 5-substituted 2-alkylidene-3-cyclopentenone products was obtained with Pt(0), but the (*S*)-enantiomer was formed when Rh(I) metal was used to promote the reaction. Our calculations suggest that the rate-determining step in both cases consists of a C−C coupling between the vinyl end of the vinylallene substrate and carbon monoxide that is accompanied by charge transfer from the metal center to the organic substrate. The reason that the two metals give different enantiomer products lies in the very different geometries of the metal centers in the transition state. The platinum center adopts a square-planar geometry throughout the C−C coupling reaction, which forces the carbonyl to migrate from the metastable, pseudoaxial position into the equatorial plane. During this migration, the carbonyl encounters the spatial constraints caused by the asymmetric DuPHOS ligand, while the vinylallene fragment is pushed away from the metal center. Thus, regardless of the steric demands of the organic substrate, the transition state that places the vinyl in a position that allows the CO to move into the sterically less crowded side of the molecule is preferred. Rh, on the other hand, maintains a square-pyramidal geometry throughout the reaction, keeping the CO ligand at the axial coordination site. The C−C coupling is accomplished by pulling the vinylallene substate closer to the metal and, as a result, the transition state that causes the least amount of steric clashes between the substrate and the DuPHOS ligand is favored, which affords the (*S*)-enantiomeric product.

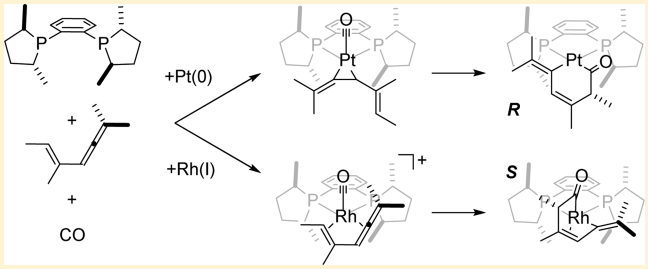

INTRODUCTION

Transition-metal-catalyzed multicomponent cycloaddition is a powerful approach to constructing complex polycyclic systems[1−3] that allows for accessing complicated molecular scaffolds with multiple stereocenters expeditiously, while preserving atom- and step-economy.[4−7] Specifically, the assembly of five-membered carbocycles has attracted much attention, in part, because they are ubiquitous in natural products of pharmaceutical importance; transition-metal-mediated [2 + 2 + 1][8−17] and [3 + 2][18−38] cycloadditions have been particularly successful. In comparison, [4 + 1] reactions[39−49] are underdeveloped, with the asymmetric [4 + 1] cycloaddition of vinylallenes and CO to afford 5-substituted 2-alkylidene-3-cyclopentenones reported by Murakami and Ito[39] being one of the most intriguing representatives of this reaction class. In this study, Rh(I) and Pt(0) were added to a chiral diphosphine ligand, (*R*,*R*)-Me-DuPHOS (1,2-bis(2,5-dimethylphosphorano)benzene) to obtain different enantiomers: Rh(I) gave the (*S*)-configuration of the cyclized product, whereas the (*R*)-isomer was obtained when Pt(0) was used.

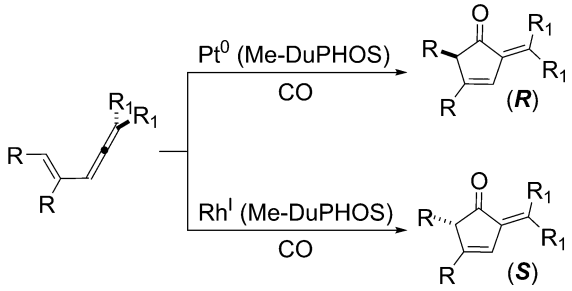

Whereas the enantioselectivity seen with the rhodium catalyst was dependent on the substituents of the allene-ene substrate,

Received: April 9, 2014
Published: May 19, 2014

dx.doi.org/10.1021/ja503427f | J. Am. Chem. Soc. 2014, 136, 9414−9423

changing the chirality of the product simply as a function of the metal identity is conceptually intriguing and practically useful. Unfortunately, the origin of this differential stereoinduction remains poorly understood to date.[50]

The original rationale proposed that the enantioselection occurs at a different point of the catalytic cycle for the two metal systems. As illustrated in Scheme 1, it was envisioned that

Scheme 1

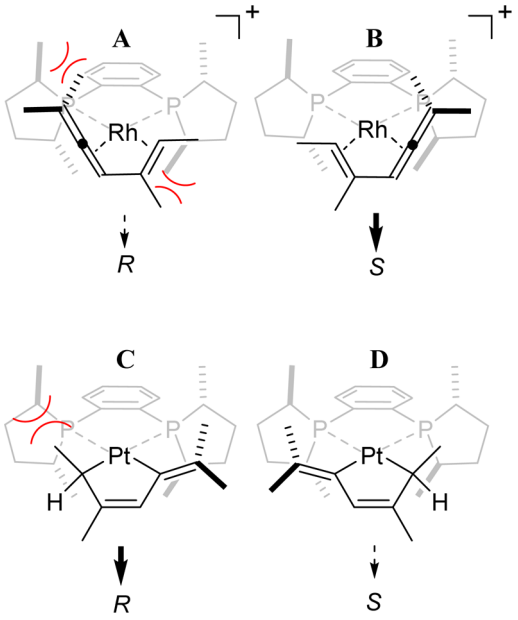

the chiral Me-DuPHOS ligand bound to Rh(I) would lead to an energetically favorable η^4-binding in the case of complex **B**, where the sterically demanding substituent on the allene moiety points to the sterically more accommodating molecular quadrant, unlike in the isomeric complex **A**, where the steric demands of the substrate molecule are mismatched with the asymmetric conformation of the DuPHOS ligand. Addition of a carbonyl to the axial position of the Rh center, followed by C−C coupling in complex **B** may give the (*S*)-cyclopentenone product. If Pt(0) is used, the corresponding η^4-complex is expected to rapidly undergo oxidative addition to give a planar σ^2-bonded platinacyclopentene, as the Pt(0) is much more reducing than Rh(I). Two configurations, denoted as complexes **C** and **D** in Scheme 1, are possible, and it was thought that the steric demands of the DuPHOS ligand would disfavor again the adduct that would lead to the (*R*)-cyclopentenone upon C−C coupling with the metal-bound carbon mononoxide (not shown in Scheme 1). But in this case, the sterically induced energy penalty would give rise to a faster cyclization and, thus, afford the (*R*)-product in greater quantities.

To test this intriguing hypothesis and better understand the mechanism of stereoinduction, we applied density functional theory (DFT) to construct complete catalytic cycles for both the Pt- and Rh-mediated reactions.[51−59] The opportunity to compare two otherwise identical Rh/Pt systems that promote the same reaction, but with reversed stereochemical preference, is promising to reveal interesting insight into what is common and what is specific to the Pt and Rh systems, both very common metals in asymmetric catalysis. To reduce the computational cost, we have used a slightly modified model system, where the R-substituents of the vinylallene were replaced with methyl groups. The chiral support ligand Me-DuPHOS is used without any simplifications. Murakami found that the absolute configuration of the product cyclopentenone does not depend on the type of vinylallene and that reversal of induced chirality is observed with various vinylallenes. Thus, we expect our simplified model to be representative and sufficiently accurate to at least capture the main components of the catalysis.

COMPUTATIONAL DETAILS

All calculations were carried out using DFT[60] as implemented in the Jaguar 7.0 suite of ab initio quantum chemistry programs.[61] Geometry optimizations were performed with the B3LYP[62−66] functional and the 6-31G** basis set. Pt and Rh were represented using the Los Alamos LACVP[67−69] basis that includes relativistic effective core potentials. The energies of the optimized structures were reevaluated by additional single point calculations on each optimized geometry using Dunning's correlation consistent triple-ζ basis set cc-pVTZ(-f)[70] that includes a double set of polarization functions. For Rh and Pt, we used a modified version of LACVP, designated as LACV3P, in which the exponents were decontracted to match the effective core potential with triple-ζ quality. Solvation energies were evaluated by a self-consistent reaction field (SCRF)[71−73] approach based on accurate numerical solutions of the Poisson−Boltzmann equation. In the results reported, solvation calculations were carried out with the 6-31G**/LACVP basis at the optimized gas-phase geometry employing the dielectric constants of ε = 7.54 for dimethoxyethane and 9.1 for dichloromethane. As is the case for all continuum models, the solvation energies are subject to empirical parametrization of the atomic radii that are used to generate the solute surface. We employed the standard set of optimized radii in Jaguar for H (1.150 Å), C (1.900 Å), P (2.074 Å), O (1.600 Å), Rh (1.464 Å), and Pt(1.377 Å). Analytical vibrational frequencies within the harmonic approximation were computed with the 6-31G**/LACVP basis to confirm proper convergence to well-defined minima or saddle points on the potential energy surface.

The energy components have been computed with the following protocol. The free energy in solution phase G(sol) has been calculated as follows:

$$G(\mathrm{sol}) = G(\mathrm{gas}) + G(\mathrm{solv}) \quad (1)$$

$$G(\mathrm{gas}) = H(\mathrm{gas}) - TS(\mathrm{gas}) \quad (2)$$

$$H(\mathrm{gas}) = E(\mathrm{SCF}) + \mathrm{ZPE} \quad (3)$$

$$\Delta E(\mathrm{SCF}) = \sum E(\mathrm{SCF})\ \text{for products} - \sum E(\mathrm{SCF})\ \text{for reactants} \quad (4)$$

$$\Delta G(\mathrm{sol}) = \sum G(\mathrm{sol})\ \text{for products} - \sum G(\mathrm{sol})\ \text{for reactants} \quad (5)$$

G(gas) is the free energy in gas phase, G(solv) is the free energy of solvation as computed using the continuum solvation model, H(gas) is the enthalpy in gas phase, T is the temperature (328 K), S(gas) is the entropy in gas phase, E(SCF) is the self-consistent field energy, i.e., "raw" electronic energy as computed from the SCF procedure, and ZPE is the zero point energy. Note that by entropy here we refer specifically to the vibrational/rotational/translational entropy of the solute(s); the entropy of the solvent is incorporated implicitly in the continuum solvation model. To locate transition states, the potential energy surface was first explored approximately using the linear synchronous transit (LST) method,[74] followed by a quadratic synchronous transit (QST)[75] search using the LST geometry as an initial guess. IRC (intrinsic reaction coordinate)[76−78] scans were performed to verify that the transition states connect to appropriate reactants and products.

dx.doi.org/10.1021/ja503427f | J. Am. Chem. Soc. 2014, 136, 9414−9423

RESULTS AND DISCUSSION

When constructing a reliable computer model of complex catalytic reactions, it is important to consider all plausible structures that are accessible at normal conditions, because they may enable different reaction pathways, possibly changing the overall outcome of the reaction decisively. Hence, a large number of possible structures must be explored carefully to identify plausible catalyst/substrate geometries that are most consistent with both experimental and theoretical considerations. As suspected previously based on chemical intuition alone, the η^4-bound π-complex of the [Pt(0)-vinylallene] does not exist according to our calculations, i.e., such a complex does not constitute a proper minimum on the potential energy surface (PES). Surprisingly, the κ^2-bound σ-complex (**C** and **D** in Scheme 1) is not the lowest energy structure despite similar compounds having been crystallographically characterized.[79] Instead, our extensive sampling of the PES revealed that the lowest energy structure for complex **1** is obtained by binding the vinylallene substrate in a η^2-fashion, as shown in Figure 1.

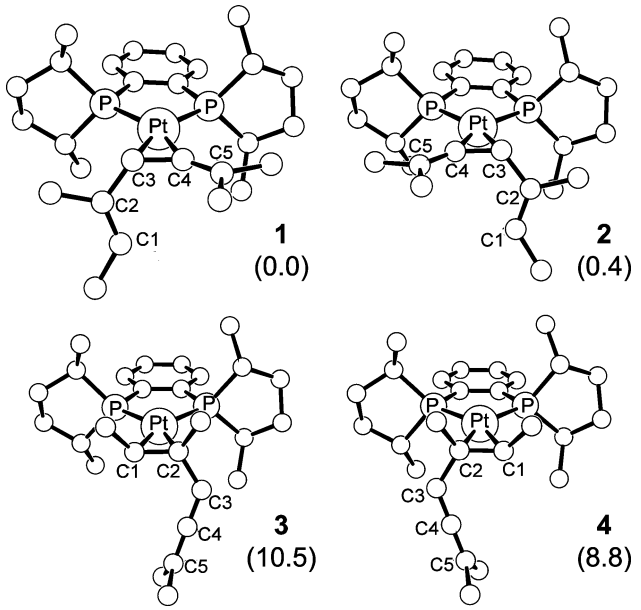

Figure 1. Reactant structures. Relative solution-phase free energies in kcal/mol are given in parentheses.

The stereochemistry of the (*R*,*R*)-Me-DuPHOS backbone gives rise to diastereomer **2**, which is practically isoenergetic with **1** at a relative solution-phase free energy of 0.4 kcal/mol. As the formation of the platinacyclopropene-like ring forces the substrate molecule into a pseudoplanar orientation with respect to the molecular plane formed by the diphosphine and Pt moieties, the asymmetric spatial compartments of the DuPHOS ligand make little to no discrimination of these two diastereomers. We also considered the regioisomers **3** and **4**, where the vinylic end of the substrate is bound to the Pt-center; they are 10.5 and 8.8 kcal/mol higher in energy than **1**, respectively. This observation is in good agreement with the intuitive expectation that the distal end of the allene moiety should be a better π-base than the vinyl group.

Inspection of the geometric parameters of **1** and **2**, in particular the C3−C4−C5 angles of the allene (about 140° compared to 180° in the free allene), illustrates that these adducts are not simply π-complexes but contain a significant contribution from a bidentate σ-description of bonding, which introduces an electronic structure consistent with an oxidative addition process of Pt(0) to Pt(II). The square-planar environment surrounding platinum with the C3−C4 bond distance being notably elongated at 1.433 Å in **1** compared to 1.317 Å in free vinylallene supports this hypothesis, as these structural features are consistent with transfer of electron density from d_{x2-y2} of the electron-rich Pt(0) center to the π^* orbital of the allene moiety. The notion that allene binding to d^{10} Pt(0) contains some amount of oxidative addition is well appreciated. For example, Osborn concluded based on NMR data that the structure was more like metallacyclopropane, with platinum being in the formal oxidation state (II).[80] Subsequent work has provided further support for this interpretation of how allene binds to electron-rich metal centers.[81,82]

Pt(0)−Me-DuPHOS-Catalyzed Cyclization. Figure 2 shows the mechanism that is most consistent with our DFT

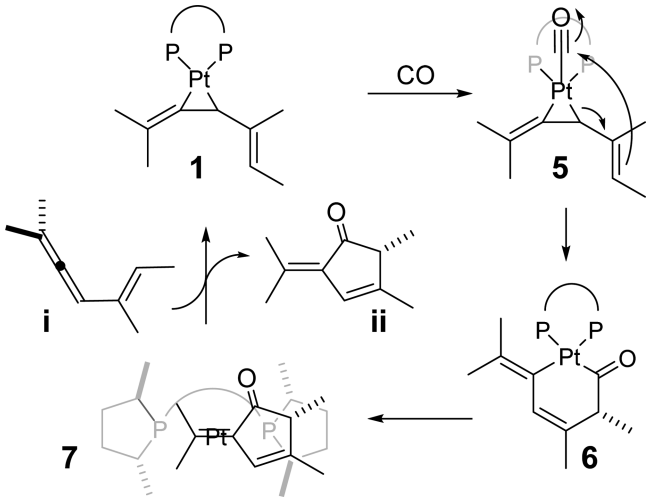

Figure 2. Catalytic cycle for [4 + 1] cycloaddition of vinylallene and CO affording (*R*)-cyclopentenone.

calculations. The catalytic cycle starts with the resting state complex **1** binding CO to afford a square-pyramidal five-coordinate 18-electron species **5**. This intermediate can choose from several plausible reaction pathways, as we conceptualize in Figure 3: The heterolytic cleavage of the Pt−C bond gives rise to a negatively charged carbon center, as illustrated in **5a**, which

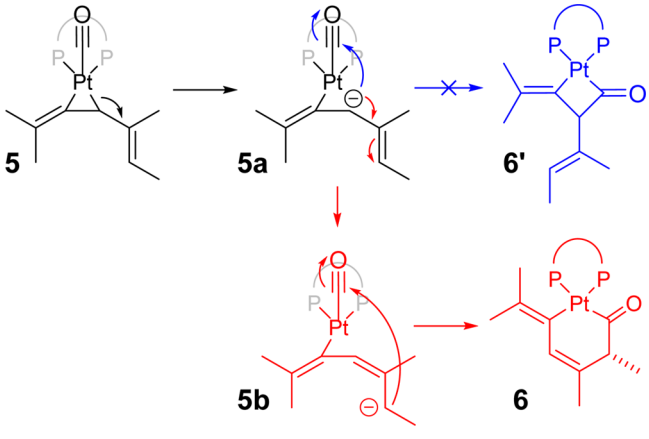

Figure 3. Plausible pathways from intermediate **5**.

dx.doi.org/10.1021/ja503427f | J. Am. Chem. Soc. 2014, 136, 9414−9423

can either perform a nucleophilic attack on the carbonyl carbon to afford the insertion product platinacyclobutenone **6′** or place the negative charge through resonance on the terminal vinylic carbon, as shown in **5b**. Nucleophilic attack on the carbonyl may form the relaxed six-membered platinacyclohexenone intermediate **6**. It is important to realize that although we can envision the overall rearrangement from **5** to **6** in a stepwise manner via hypothesized species **5a** and **5b**, the transformation of **5** to **6** will likely be a concerted process without any zwitterionic intermediates being formed. Reductive elimination from **6** gives the product-complex **7**, which completes the catalytic cycle by releasing the cyclopentenone product. The alternative pathway via intermediate **6′** is unproductive, as it is associated with unreasonable barriers that are 16 kcal mol^{-1} higher in energy than **5-TS**. These putative reaction profiles are presented in the Supporting Information and will not be discussed further.

Figure 4 illustrates the computed reaction free energy profiles for the proposed mechanism. The formation of (*R*)-cyclopentenone, which is experimentally seen to be the major product, is shown as a solid blue line, whereas the profile for forming the minor enantiomeric product (*S*)-cyclopentenone is drawn using a broken line. Carbon monoxide binding to form the reactant complexes **5** and **8** is thermodynamically uphill by about 13 kcal/mol. Although we did not locate the transition state for CO binding because this step is expected to be dominated by translational entropy changes, which cannot be modeled properly with standard quantum chemical methods that only sample the electronic surface, this step is most likely rapid. Complexes **5** and **8** subsequently undergo migratory insertion to form intermediates **6** and **9**, traversing the transition states **5-TS** and **8-TS**, respectively. As will be highlighted below, this step is unusual in the sense that the ring-expanding reorganization and insertion of carbonyl are intrinsically coupled to each other and occur in a concerted fashion. The free energies of activation for this step are 23.7 and 24.8 kcal/mol, respectively, for the two enantiomers. These energies are very plausible given the conditions at which the reaction is observed, namely at a mildly elevated temperature of 55−60 °C and with a reaction time of 6−20 h. Finally, the intermediates **6** and **9** may undergo reductive eliminations that are associated with barriers of 17.1 and 19.2 kcal/mol to afford the final product complexes **7** and **10**, respectively. Therefore, the insertion step is likely to be rate-determining for both reaction pathways. The transition state **8-TS** for the insertion leading to the (*S*)-isomer is higher by 1.1 kcal/mol in solution-phase free energy, with the electronic energy component ΔE(SCF) being 1.9 kcal/mol higher than **5-TS**, which gives the (*R*)-isomer. These energy differences are in agreement with the experimental observation that the (*R*)-isomer is the major product for all vinylallenes examined, but the observed enantiometic excess (ee) is only moderate at ∼70%.[39] Thus, our calculated reaction energy profiles suggest that enantioselectivity of the overall cycloaddition reaction is determined during the insertion step that is coupled to the metallacycle expansion. The proposal mentioned above is therefore correct in that the carbonyl insertion is rate-determining, but the stereoinducing feature that relied on sterical demands of the presumed κ^2-bound σ-complex (**C** and **D** in Scheme 1) cannot be confirmed in our calculations. Nonetheless, our calculations indicate a modest energy difference between the two possible pathways, resulting in the different enantiomeric products that can be examined in greater detail.

The structural features of the transition states **5-TS** and **8-TS** are highlighted in Figure 5. To understand how the chiral information is propagated from the asymmetric Me-DuPHOS backbone into the vinylallene substrate, we divided the coordination space presented by the C_2-symmetric (*R*,*R*)-Me-DuPHOS into four quadrants as shown in Figure 5. The space in quadrants 1 and 3 is encroached by the methyl groups of Me-DuPHOS, whereas quadrants 2 and 4 are largely empty with the methyl moieties pointing away. Consequently, quadrants 1 and 3 are sterically crowded, whereas quadrants 2 and 4 are more accommodating to additional ligand fragments spatially, as we denote by + and − signs, respectively. A close analysis of the transition state structures reveals that the M−CO fragment becomes significantly bent to engage in the insertion reaction, as the carbon atom of CO ligand changes its hybridization from sp to sp^2. As a result, the carbonyl-oxygen atoms in **5-TS** and **8-TS** must point toward the Me-DuPHOS backbone, thereby reaching spatially into the aforementioned coordination quadrants 1 and 3, respectively. In **5-TS** this bending motion can be accommodated without any sterically induced energy penalties within the quadrants 2 and 4. Thus,

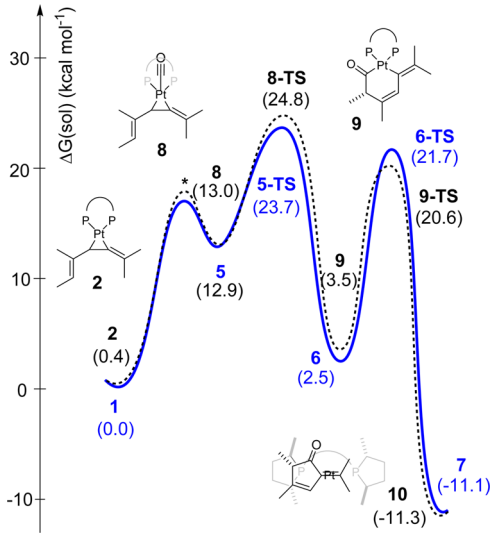

Figure 4. Computed free energy profiles of our proposed cycloaddition pathway. Transition states indicated by * were not explicitly located.

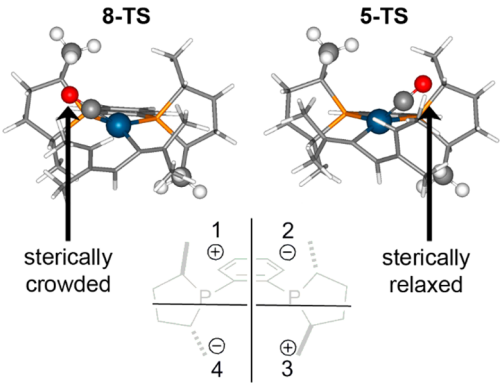

Figure 5. Calculated geometries of the transition states leading to the two diastereomers for the insertion pathway.

dx.doi.org/10.1021/ja503427f | J. Am. Chem. Soc. 2014, 136, 9414−9423

the steric clash between the bending carbonyl and the methyl group of the Me-DuPHOS backbone, as illustrated in Figure 5, provides a simple explanation for the modest energetic preference of **5-TS** over **8-TS**. This hypothetical reasoning is able to address an important feature reported by Murakami et al. for Pt-Me-DuPHOS-catalyzed [4 + 1] cycloaddition, namely, that the observed ee of the (*R*)-cyclopentenone is not significantly affected by the structures of the vinylallene reactants. The ee values range between 65% and 75% for different vinylallenes, which suggests only a modest energetic difference of the two transition states, as our computations confirm. Whereas one may argue that the computational protocol employed here has an intrinsic methodological uncertainty and we may question whether DFT is good enough to capture energetic differences in this small order of magnitude, we believe that the energy difference of 1−2 kcal/mol found here is meaningful, as the classical steric argument presented above is conceptually reasonable and is confirmed within our DFT framework.

Even though our model explains the experimental findings of Murakami and Ito, it is instructional to compare our proposal with the originally postulated mechanism in greater detail. Therefore, we evaluated the originally envisioned mechanism more faithfully, as shown in Figure 6. As mentioned above, we

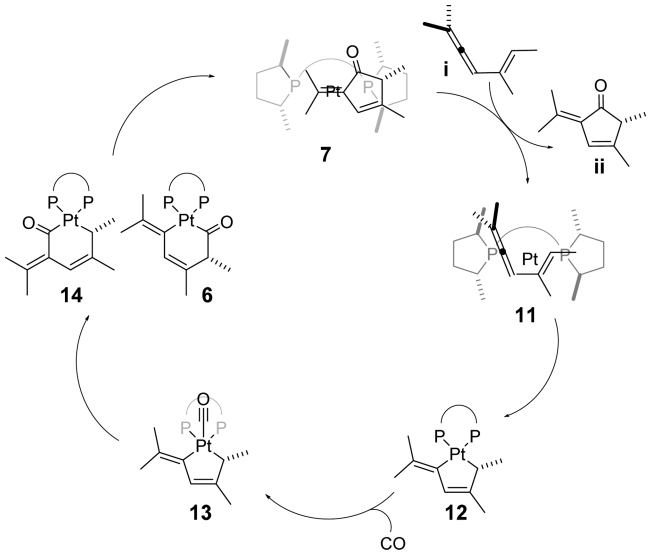

Figure 6. Catalytic pathway proposed by Murakami and Ito.

were unable to locate the η^4-bound intermediate **11**, as in all of our attempts we converged to **12**. This finding is not surprising because oxidation of the electron-rich Pt(0)-d^{10} metal center is expected to be facile. However, intermediate **12** is about 22 kcal mol^{-1} higher in free energy than **4**, precluding the mechanistic relevance of the former. In any case, we calculated the reaction energy profile of the putative cycloaddition pathway via complex **12**, leading to the experimentally observed (*R*)-cyclopentenone, and the reaction profile is shown in Figure 7. Addition of CO followed by insertion from this intermediate is reasonable at first sight. The barriers measured from **12** are 22.3 and 24.7 kcal/mol for insertion of carbonyl into the Pt−C(sp^3) and Pt−C(sp^2) bonds, respectively. However, it is important to recognize that this potential energy surface is not accessible, as the putative intermediate **12** can be considered to be in equilibrium with the energetically more favorable complex **4**. As

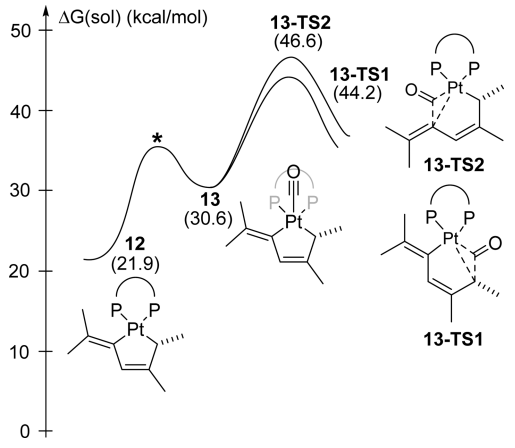

Figure 7. Computed free energy profiles of cycloaddition of vinylallene with CO affording (*R*)-cyclopentenone starting from platinacyclopentene intermediate. Transition state indicated by * was not explicitly located.

mentioned above, this κ^2-bound Pt(II) complex **12** is 22 kcal/mol higher in energy than its η^2-bound analogue **4**. Thus, the originally envisioned mechanism is only viable if **12** were the correct reference state, i.e., the lowest point in the reaction profile, which it is not, as our calculations demonstrate. The original hypothesis of the involvement of platinacyclopentene in cycloaddition was based on the isolation and crystallographic characterization of a similar intermediate when a different vinylallene substrate and a different diphosphine ligand were chosen. Treatment of $Pt(cod)_2$ in the presence of a different vinylallene (5-methyl-2-phenyl-1,3,4-hexatriene) and diphosphine dppe (1,2-bis(diphenylphosphino)ethane) led to isolation of planar platinacyclopentene **16** (shown in Figure 8) in

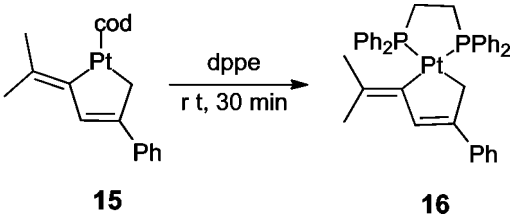

Figure 8. Experimentally isolable planar platinacyclopentene **16**.[79]

CH_2Cl_2.[79] Table 1 summarizes the results of a systematic study to better understand the equilibrium between platinacyclopropane and platinacyclopentene intermediates as the allene

Table 1. Equilibria for Different Vinylallenes and Diphosphine Backbone Ligands

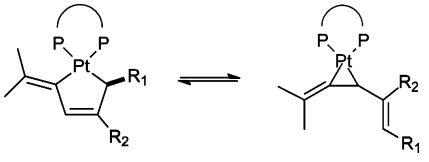

entry	R_1	R_2	P−P	ΔE(SCF) (kcal/mol)
1	H	Ph	dppe	1.7
2	H	Ph	Me-DuPHOS	−2.4
3	H	H	Me-DuPHOS	−6.3
4	Me	H	Me-DuPHOS	−13.9

dx.doi.org/10.1021/ja503427f | J. Am. Chem. Soc. 2014, 136, 9414−9423

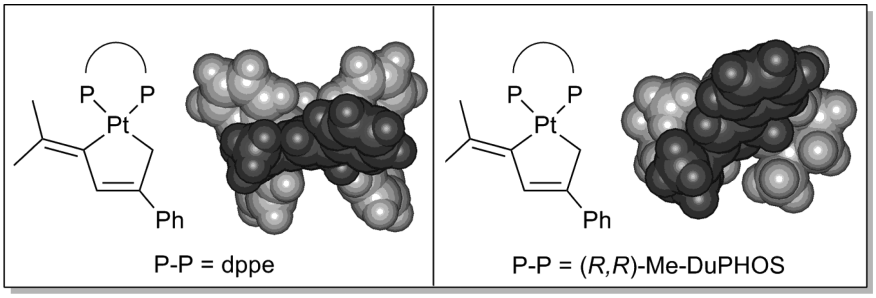

Figure 9. Role of diphosphine in stabilizing platinacylcopentene.

substitution and phosphine ligands are varied. Entry 1 shows the computed energy difference between them to be 1.7 kcal/mol favoring **16**. Both of these intermediates may therefore be catalytically relevant, as an equilibrium should exist with both structures being present in significant quantities.

This energy difference is consistent with the experimental observation that complex **16** can be isolated. To quantify the role of the backbone in determining the energies of the isomers in equilibrium, we replaced dppe with Me-DuPHOS (entry 2) and found that the equilibrium shifts in favor of platinacyclopropane by about 4 kcal/mol, which we attribute to the lack of ligand flexibility in this ligand. As shown in Figure 9, the dppe phenyl rings can reorient to create a pocket that accommodates the platinacyclopentene, unlike in the Me-DuPHOS ligand, where the diphosphine scaffold is much more rigid. Consequently, the Me-DuPHOS ligand cannot undergo the energetically costly torquing motion to generate a more accommodating binding pocket for the metallacycle. As a result, the platinacyclopentene structure becomes increasingly difficult to access when moving from dppe to the Me-DuPHOS backbone ligand. As demonstrated in entry 3 of Table 1, the preference of the platinacyclopropene isomer can be further increased by about 4 kcal/mol by exchanging the phenyl group at R_2 position for H, which is due to the loss of extended π-conjugation. Finally, introduction of methyl at the R_1 position distorts the equilibrium further in favor of the three-membered ring to about 14 kcal/mol (entry 4 in Table 1). These explicitly calculated relative energies highlight the fact that the platinacyclopentene isomer was isolated using the dppe ligand and that the phenyl-substituted allene substrate cannot be used to make reliable assumptions about which isomer should be dominant when the simpler alkyl-substituted allene substrate is used in combination with the less flexible Me-DuPHOS ligand. In conclusion, the equilibrium between the two isomeric forms of the reactant adduct shows an interesting, and unexpectedly great, dependence on both the composition of the substrate and the nature of the backbone diphosphine ligand. Judicious choice of the substrate/ligand combination may therefore allow for much greater control over which mechanism is operational. This insight may provide a rationally exploitable platform in future optimizations of the Pt-based [4 + 1] carbocyclizations; work toward substantiating this idea is in progress in our laboratory.

Rh(I)−Me-DuPHOS-Catalyzed Cyclization. With the new mechanistic proposal for the Pt-complex at hand, the question of how to reverse the stereochemical outcome using the same diphosphine ligand and changing the metal becomes more intriguing. Nothing about the mechanism discussed above points to a direct, unusual role of the Pt-center that may explain the reversed stereochemical outcome in a straightforward fashion. Figure 10 depicts the most plausible reaction pathway for cycloaddition using the cationic Rh(I)−(Me-DuPHOS)

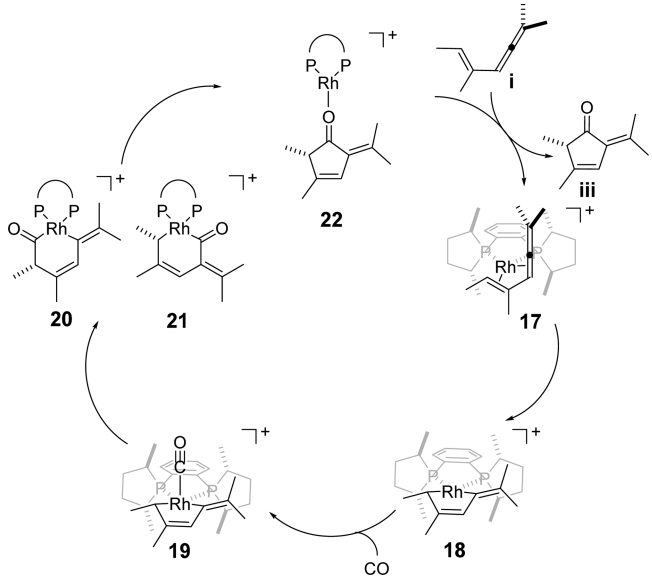

Figure 10. Rh−Me-DuPHOS-catalyzed cycloaddition pathway affording (*S*)-cyclopentenone.

system. The catalysis starts with η^4-bound species **17** followed by oxidative addition, CO addition, migratory insertion, and reductive elimination. The corresponding energy profiles are shown in Figure 11. The optimized geometries of mechanistically important intermediates and transition states are illustrated in Figures 12 and 14. Unlike in the case of Pt(0), Rh(I) does not undergo smooth oxidative addition to Rh(III) to form rhodacyclopentene **18** after vinylallene binding. Instead, the catalyst−substrate π-adduct **17** is formed with a slightly activated vinylallene moiety displaying bond distances of 1.393 Å (C1−C2), 1.459 Å (C2−C3), and 1.388 Å (C3−C4), as illustrated in Figure 12. The fact that the reactant π-adduct can be formed with Rh(I), while Pt(0) spontaneously gives the σ-complex is easy to understand, as Pt(0) is much easier to oxidize than Rh(I). The ultimate consequence of this difference is, however, much more difficult to see. Interestingly, the Rh(I) center does not even undergo oxidative addition to form the rhodacyclopentene fragment, as one may have anticipated based on the Pt-based reaction mentioned above. Instead, the π-adduct **17** binds a CO ligand to afford intermediate **19**, where the vinylallene becomes more activated with calculated bond lengths being 1.427 Å (C1−C2), 1.423 Å (C2−C3), and 1.429 Å (C3−C4). The C−C−C bond angle of the allenic moiety changes from 151.6° in **17** to 139.1° in **19**.

dx.doi.org/10.1021/ja503427f | J. Am. Chem. Soc. 2014, 136, 9414−9423

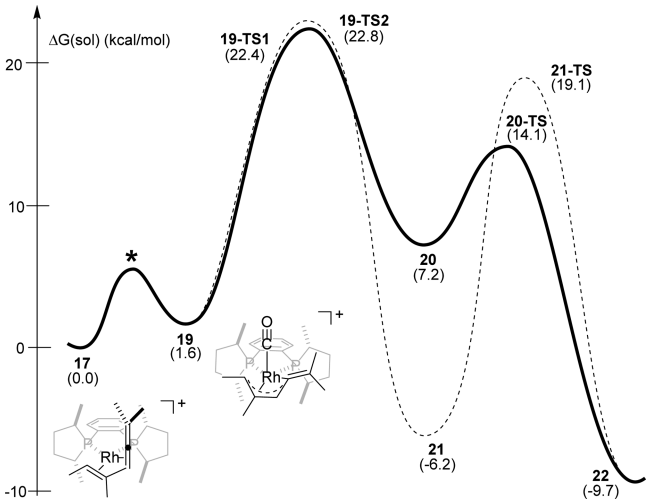

Figure 11. Computed free energy profiles of Rh–Me-DuPHOS-catalyzed cycloaddition of vinylallene and CO, leading to the formation of (*S*)-cyclopentenone. Transition state indicated by * was not explicitly located.

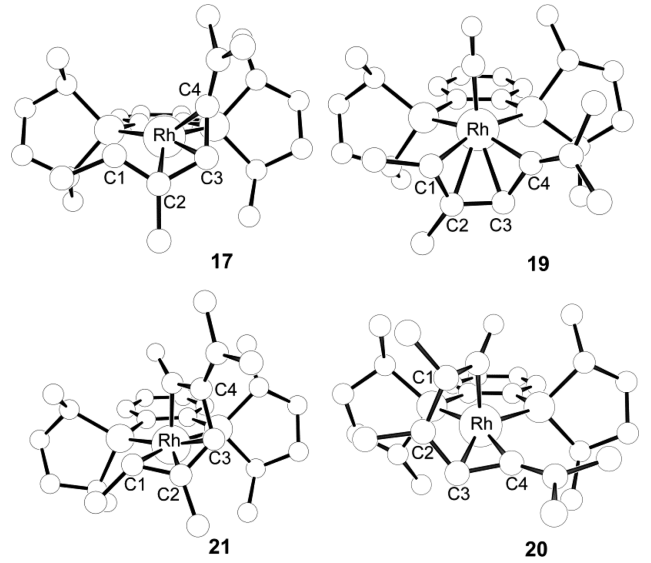

Figure 12. Optimized geometries of the intermediates encountered in the Rh-catalyzed cyclization.

Thus, complex **19** begins to acquire the electronic structure pattern of a rhodacyclopentene moiety to a much greater extent than **17** but is still a η^4-bound π-complex, as indicated by the geometry shown in Figure 12. The catalytic cycle continues with a somewhat surprising step where the migratory insertion of CO into the Rh–C bond and the anticipated oxidative addition to formally reduce the allene moiety are coupled and executed in a concerted fashion. The carbonyl ligand has a choice to insert into either the olefinic or allenic carbon–Rh bonds to form the regioisomeric intermediates **20** and **21**. Kinetically, both pathways are identical, with the transition states **19-TS1** and **19-TS2** being nearly isoenergetic at 22.4 and 22.8 kcal mol^{-1}. Intermediate **20** is much less preferred, however, than **21**, with the latter being a thermodynamic trap, as highlighted in Figure 11. Intermediate **21** is much lower in energy than **20** because the π-component of the carbonyl can engage in significant π-conjugation, as highlighted in Lewis structures shown in Figure 10. Moreover, inspection of the optimized geometries indicate that the carbonyl maintains its axial binding site in the square-pyramidal coordination geometry of the Rh(III)-center and, as a consequence, forces the alkylidene (=CMe_2) moiety to orient away from the sterically demanding parts of the Me-DuPHOS backbone ligand. In complex **20**, the alkylidene fragment is in closer contact with the diphosphine ligand, causing additional energy penalties, as illustrated in Figure 12. Reductive elimination, accompanied by C–C bond formation, constitutes the last step of the catalytic cycle and yields the final product complex **22**. Note that the two divergent pathways involving intermediates **20** and **21** converge at this step to form the same product. Interestingly, the thermodynamically less favorable intermediate **20** can reductively eliminate much more readily, with the transition state **20-TS** being only 7 kcal mol^{-1} higher in energy. The more stable regioisomer **21** must traverse an analogous transition state **21-TS** at 19.1 kcal mol^{-1}. Thus, the activation free energy for this step is 25.3 kcal mol^{-1}, which is nearly 3 kcal mol^{-1} higher in energy than the oxidative addition step, identified thus far as being the most difficult step. This bifurcation in the potential energy surface will result in a complex overall kinetics; depending on the initial internal momentum and vibrational mode distribution of the intermediate **19**, which will be nontrivially correlated to the specific reaction conditions, the reaction may progress through intermediate **20** or **21**. In the former case, the rate-determining barrier is 22.4 kcal mol^{-1} and is associated with **19-TS1**, whereas in the latter case the rate-determining barrier is 25.3 kcal mol^{-1}.

Figure 13 depicts the energy profiles of the cycloaddition pathways resulting from vinylallene binding to the Rh center from the other face. Not surprisingly, the overall mechanism is identical to what was seen for the formation of the (*S*)-cyclopentenone, but the lowest energy barrier, which is associated with the migratory insertion coupled to the oxidative addition, is found at 25.2 kcal mol^{-1}, which is nearly 2.5 kcal mol^{-1} higher than what was seen for the (*S*)-cyclopentenone. These calculated energies are in good agreement with the (*S*)-enantiomer being the major isomer observed experimentally. Whereas this finding is in agreement with the experimental finding qualitatively, the transition state energy difference is too large to be in quantitative agreement with the observation of 40–60% ee that was typically found experimentally.[39] Thus, our computer simulations reproduce the experimentally observed switch in the enantioselectivity of the reaction as a function of the identity of the metal reasonably well to encourage a more detailed analysis of the reason for this switch.

The side view of the calculated transition state structures shown in Figure 15 along with the selected bond distances and angles in Table 2 illuminate the most important structural difference that governs the enantioselectivity; platinum maintains a square planar geometry, as indicated in Figure 15 both for **5-TS** and **8-TS**, which is not surprising for a Pt(II)-d^8 center and suggests that the formal oxidation of the Pt(0) center has long been completed at the transition state. Thus, the migratory insertion component of this concerted transition state consisting of insertion and platinacycle expansion is the dominating feature at the transition state. The consequence of this electronic structure is that the vinylallene moiety is pushed away from the [DuPHOS-Pt] fragment, as indicated by a Pt–C1 distance of 3.633 Å in **5-TS**. Therefore, it is the migrating carbonyl that causes the steric clash with the asymmetric DuPHOS ligand and not the vinylallene fragment. In the

dx.doi.org/10.1021/ja503427f | J. Am. Chem. Soc. 2014, 136, 9414–9423

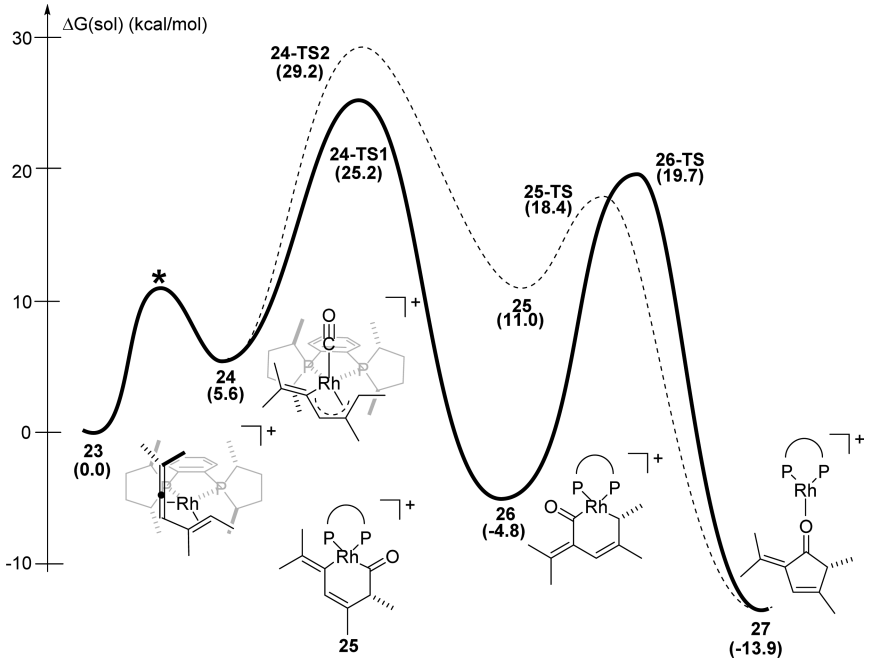

Figure 13. Computed free energy profiles of Rh−Me-DuPHOS-catalyzed cycloaddition of vinylallene and CO affording (*R*)-cyclopentenone. Transition state indicated by * was not explicitly located.

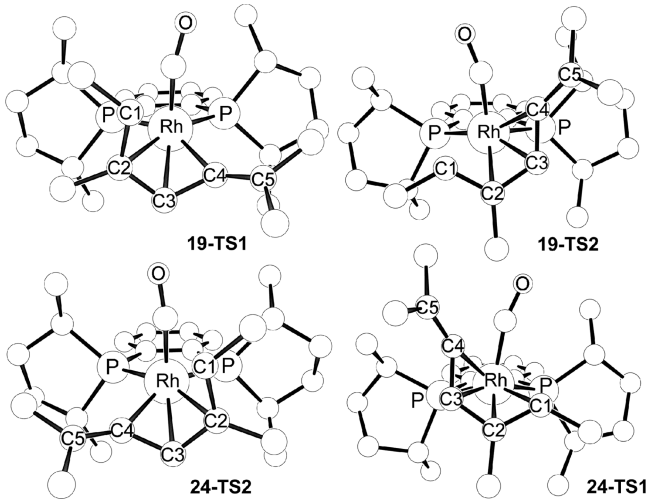

Figure 14. Calculated structures of the four transition states of the Rh-catalyzed carbocyclization.

energetically preferred transition state **5-TS**, the carbonyl occupies a much more accommodating quadrant than in **8-TS**, as discussed above. The rhodium center has also completed the redox component of the reaction at the transition state and is most appropriately described as a Rh(III) center, which prefers a five-coordinate geometry around the metal. In both **24-TS1** and **19-TS1** the rhodium center adopts a square-pyramidal geometry with the carbonyls occupying the axial ligand positions. The C−C coupling is accomplished by pulling the vinyl portion of the vinylallene substrate closer to the [DuPHOS-Rh] fragment, illustrated by a much shorter Rh−C1 distance of 2.545 Å in **19-TS1**; thus, in this case, it is the vinylallene that performs the migratory motion and encounters the spatially discriminating compartments of the DuPHOS ligand. Note that that the classical, intuitive rationale of the stereochemical outcome relies on the steric demands of the vinylallene ligand only, ignoring the CO ligand. This assumption is reasonable in the Rh case, as we show above. In the Pt case, however, the CO ligand must be considered, as it is the dominant ligand interacting with the DuPHOS ligand.

■ CONCLUSIONS

Scheme 2 summarizes our findings and highlights the mechanistic differences between the Pt and Rh catalyzed [4 + 1] carbocyclizations leading to the production of the (*R*)- and (*S*)-enantiomers, respectively. Previously, it was proposed that Pt(0) engages in oxidative addition with the vinylallene substrate spontaneously to afford a platinacyclopentene intermediate, while Rh was envisioned to form a π-complex. We found that the κ^2-bound platinacyclopentene intermediate is too high in energy to be accessible under normal conditions. Instead, the reactant is η^2-bound to the Pt center, with the metal developing some Pt(II) character, i.e., donating a significant amount of electron density to the allenic π^*-orbital. This binding motif places the sterically demanding substituents of the vinyl moiety relatively far away from the stereodirecting, asymmetric Pt-DuPHOS fragment. The transition state is dominated by the migratory insertion process, where the carbonyl ligand moves from the axial coordination site into the equatorial position. The vinylallene substrate is pushed further away from the Pt-DuPHOS fragment, thus rendering the steric demands of the vinylallene substrate less important for the stereochemical outcome. Instead, steric demands of the migrating carbonyl substrate becomes most important. This transition state characteristic is the result of the Pt(II)-d^8 center insisting on a square-planar, four-coordinate geometry. As anticipated previously, Rh(I) forms a stable π-complex with the substrate, and as the metal becomes formally oxidized to a Rh(III)-d^6 center at the stereodirecting CO insertion transition state, it maintains a tightly bound, square-pyramidal, five-coordinate geometry, with the carbonyl ligand remaining stationary at the axial position. The C−C coupling is accomplished by a migratory motion of the vinyl moiety and

dx.doi.org/10.1021/ja503427f | J. Am. Chem. Soc. 2014, 136, 9414−9423

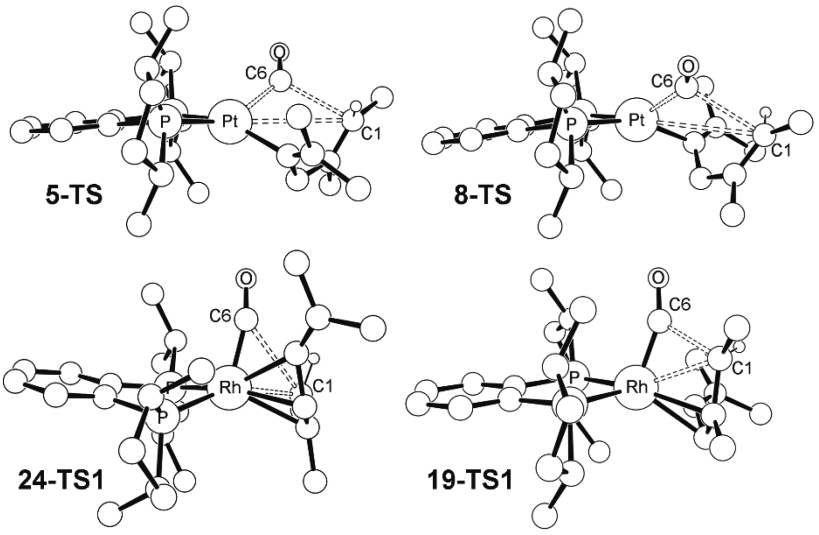

Figure 15. Calculated structures of the most relevant transition states.

Table 2. Selected Bond Lengths (Å) and Angles (deg)[a]

structure	M−C1	M−C6	C1−C6	∠ [PP]−M−(CO)
5-TS	3.633	2.138	2.365	129.4
8-TS	3.726	2.125	2.530	131.6
24-TS1	2.416	1.907	2.904	116.2
19-TS1	2.545	1.908	2.031	110.9

[a]The [PP]−M−(CO) bond angle is defined by the angle between the central point of the two phosphorus atoms, the metal, and the carbonyl carbon.

Scheme 2

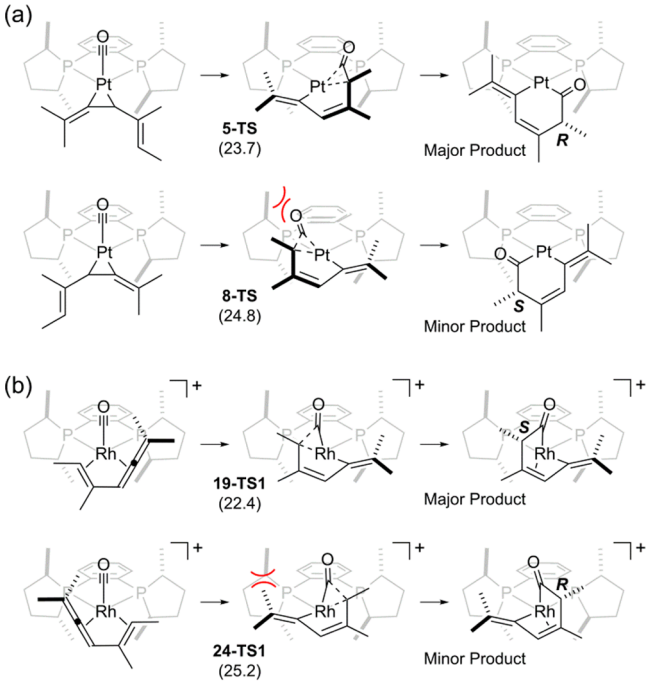

the energetic discrimination leading to the enantioselectivity is based on the steric demands of the vinylallene group, thus affording the *S*-enantiomer as the major product.

This work highlights the importance of considering the coordination geometries that a metal center prefers when performing carbocyclization reactions. Pt(II) and other d^8 metals will tend to adopt four-coordinate, square-planar geometries, such that the axial ligands will be the mobile entity, whereas Rh(III) and other d^6-systems will adopt five-coordinate, square-pyramidal or trigonal-bipyramidal geometries, where the carbonyl will maintain its axial position and force the substrate with extended π-components to be the mobile fragment. These transition states will tend to pull the substrate fragment closer to the asymmetric [M−DuPHOS] moiety, and the stereoselectivity of the reaction will be dominated by the spatial demands of the more complex π-substrate.

■ ASSOCIATED CONTENT

Supporting Information

Reaction energy profiles of additional pathways considered, additional discussion, and Cartesian coordinates of all intermediate and transition state structures discussed. This material is available free of charge via the Internet at http://pubs.acs.org.

■ AUTHOR INFORMATION

Corresponding Author

mbaik@indiana.edu.

Notes

The authors declare no competing financial interest.

■ ACKNOWLEDGMENTS

We thank the NSF (0116050, CHE-0645381, CHE-1001589), the Research Corporation (Scialog Award to M.H.B.), and the National Research Foundation of Korea for a WCU Award to Korea University (R31-2012-000-10035-0).

■ REFERENCES

(1) Curran, D. P. *Advances in Cycloaddition*; JAI Press: Greenwich, 1994.
(2) Trost, B. M. *Angew. Chem., Int. Ed. Engl.* **1995**, *34*, 259.
(3) Inglesby, P. A.; Evans, P. A. *Chem. Soc. Rev.* **2010**, *39*, 2791.
(4) Lautens, M.; Klute, W.; Tam, W. *Chem. Rev.* **1996**, *96*, 49.
(5) Ojima, I.; Tzamarioudaki, M.; Li, Z.; Donovan, R. J. *Chem. Rev.* **1996**, *96*, 635.
(6) Frühauf, H.-W. *Chem. Rev.* **1997**, *97*, 523.

(7) Leahy, D. K.; Evans, P. A. Rhodium(I)-Catalyzed Allylic Substitution Reactions and Their Applications to Target Directed Synthesis. In *Modern Rhodium-Catalyzed Organic Reactions*; Evans, P. A., Ed.; Wiley-VCH Verlag GmbH & Co. KGaA, Weinheim, 2005; p 191
(8) Knoelker, H. J.; Heber, J.; Mahler, C. H. *Synlett* **1992**, 1002.
(9) Knoelker, H. J.; Heber, J. *Synlett* **1993**, 924.
(10) Brummond, K. M.; Wan, H.; Kent, J. L. *J. Org. Chem.* **1998**, *63*, 6535.
(11) Brummond, K. M.; Kent, J. L. *Tetrahedron* **2000**, *56*, 3263.
(12) Baker, M. V.; Brown, D. H.; Skelton, B. W.; White, A. H. *J. Chem. Soc., Dalton Trans.* **2002**, 2595.
(13) Imhof, W.; Anders, E.; Gobel, A.; Gorls, H. *Chem.—Eur. J.* **2003**, *9*, 1166.
(14) Wender, P. A.; Croatt, M. P.; Deschamps, N. M. *J. Am. Chem. Soc.* **2004**, *126*, 5948.
(15) Jeong, N. In *Modern Rhodium-Catalyzed Organic Reactions*; Evans, P. A., Ed.; Wiley-VCH: Weinheim, 2005; p 215.
(16) Pérez-Castells, J. In *Metal Catalyzed Cascade Reactions*; Müller, T. J., Ed.; Springer: Berlin, 2006; Vol. *19*, p 207.
(17) Lee, H.-W.; Kwong, F.-Y. *Eur. J. Org. Chem.* **2010**, *2010*, 789.
(18) Trost, B. M. *Angew. Chem., Int. Ed. Engl.* **1986**, *25*, 1.
(19) Trost, B. M.; Chan, D. M. T. *J. Am. Chem. Soc.* **1982**, *104*, 3733.
(20) Lautens, M.; Ren, Y.; Delanghe, P. H. M. *J. Am. Chem. Soc.* **1994**, *116*, 8821.
(21) Gulías, M.; García, R.; Delgado, A.; Castedo, L.; Mascareñas, J. L. *J. Am. Chem. Soc.* **2005**, *128*, 384.
(22) Herath, A.; Montgomery, J. *J. Am. Chem. Soc.* **2006**, *128*, 14030.
(23) Lian, J.-J.; Chen, P.-C.; Lin, Y.-P.; Ting, H.-C.; Liu, R.-S. *J. Am. Chem. Soc.* **2006**, *128*, 11372.
(24) Trost, B. M.; Stambuli, J. P.; Silverman, S. M.; Schwörer, U. *J. Am. Chem. Soc.* **2006**, *128*, 13328.
(25) Trost, B. M.; Silverman, S. M.; Stambuli, J. P. *J. Am. Chem. Soc.* **2007**, *129*, 12398.
(26) Lian, Y.; Davies, H. M. L. *J. Am. Chem. Soc.* **2009**, *132*, 440.
(27) Wang, Y.-F.; Zhu, X.; Chiba, S. *J. Am. Chem. Soc.* **2012**, *134*, 3679.
(28) Dieskau, A. P.; Holzwarth, M. S.; Plietker, B. *J. Am. Chem. Soc.* **2012**, *134*, 5048.
(29) Trost, B. M.; Lam, T. M. *J. Am. Chem. Soc.* **2012**, *134*, 11319.
(30) Trost, B. M.; Silverman, S. M. *J. Am. Chem. Soc.* **2012**, *134*, 4941.
(31) Briones, J. F.; Davies, H. M. L. *J. Am. Chem. Soc.* **2013**, *135*, 13314.
(32) Nishimura, T.; Ebe, Y.; Hayashi, T. *J. Am. Chem. Soc.* **2013**, *135*, 2092.
(33) Miura, T.; Funakoshi, Y.; Murakami, M. *J. Am. Chem. Soc.* **2014**, *136*, 2272.
(34) Yamago, S.; Nakamura, E. *J. Chem. Soc., Chem. Commun.* **1988**, *0*, 1112.
(35) Yamago, S.; Nakamura, E. *Tetrahedron* **1989**, *45*, 3081.
(36) Lewis, R. T.; Motherwell, W. B.; Shipman, M. *J. Chem. Soc., Chem. Commun.* **1988**, 948.
(37) Jiao, L.; Ye, S.; Yu, Z.-X. *J. Am. Chem. Soc.* **2008**, *130*, 7178.
(38) Liang, Y.; Liu, S.; Xia, Y.; Li, Y.; Yu, Z.-X. *Chem.—Eur. J.* **2008**, *14*, 4361.
(39) Murakami, M.; Itami, K.; Ito, Y. *J. Am. Chem. Soc.* **1999**, *121*, 4130.
(40) Sigman, M. S.; Eaton, B. E. *J. Am. Chem. Soc.* **1996**, *118*, 11783.
(41) Murakami, M.; Itami, K.; Ito, Y. *J. Am. Chem. Soc.* **1997**, *119*, 2950.
(42) Murakami, M.; Itami, K.; Ito, Y. *J. Am. Chem. Soc.* **1999**, *121*, 4130.
(43) Maestri, A. G.; Cherry, K. S.; Toboni, J. J.; Brown, S. N. *J. Am. Chem. Soc.* **2001**, *123*, 7459.
(44) Son, S.; Fu, G. C. *J. Am. Chem. Soc.* **2007**, *129*, 1046.
(45) Coscia, R. W.; Lambert, T. H. *J. Am. Chem. Soc.* **2009**, *131*, 2496.
(46) Eaton, B. E.; Rollman, B.; Kaduk, J. A. *J. Am. Chem. Soc.* **1992**, *114*, 6245.
(47) Sigman, M. S.; Kerr, C. E.; Eaton, B. E. *J. Am. Chem. Soc.* **1993**, *115*, 7545.
(48) Sigman, M. S.; Eaton, B. E. *J. Org. Chem.* **1994**, *59*, 7488.
(49) Morimoto, T.; Chatani, N.; Murai, S. *J. Am. Chem. Soc.* **1999**, *121*, 1758.
(50) Meng, Q.; Li, M.; Zhang, J. *J. Mol. Struct. (THEOCHEM)* **2005**, *726*, 47.
(51) Ziegler, T. *Chem. Rev.* **1991**, *91*, 651.
(52) Niu, S.; Hall, M. B. *Chem. Rev.* **2000**, *100*, 353.
(53) Yu, Z.-X.; Wender, P. A.; Houk, K. N. *J. Am. Chem. Soc.* **2004**, *126*, 9154.
(54) Pitcock, W. H., Jr.; Lord, R. L.; Baik, M.-H. *J. Am. Chem. Soc.* **2008**, *130*, 5821.
(55) Wang, H.; Sawyer, J. R.; Evans, P. A.; Baik, M. H. *Angew. Chem., Int. Ed.* **2008**, *47*, 342.
(56) Baik, M.-H.; Baum, E. W.; Burland, M. C.; Evans, P. A. *J. Am. Chem. Soc.* **2005**, *127*, 1602.
(57) Mazumder, S.; Shang, D.; Negru, D. E.; Baik, M.-H.; Evans, P. A. *J. Am. Chem. Soc.* **2012**, *134*, 20569.
(58) Baik, M. H.; Mazumder, S.; Ricci, P.; Sawyer, J. R.; Song, Y. G.; Wang, H. J.; Evans, P. A. *J. Am. Chem. Soc.* **2011**, *133*, 7621.
(59) Williams, D. R.; Shah, A. A.; Mazumder, S.; Baik, M.-H. *Chem. Sci.* **2012**, *4*, 238.
(60) Parr, R. G.; Yang, W. *Density Functional Theory of Atoms and Molecules*; Oxford University Press: New York, 1989.
(61) *Jaguar 7.0*; Schrödinger, Inc., New York, 2013.
(62) Slater, J. C. *Quantum Theory of Molecules and Solids, Vol. 4: The Self-Consistent Field for Molecules and Solids*; McGraw-Hill: New York, 1974.
(63) Vosko, S. H.; Wilk, L.; Nusair, M. *Can. J. Phys.* **1980**, *58*, 1200.
(64) Becke, A. D. *Phys. Rev. A* **1988**, *38*, 3098.
(65) Becke, A. D. *J. Chem. Phys.* **1993**, *98*, 5648.
(66) Lee, C.; Yang, W.; Parr, R. G. *Phys. Rev. B* **1988**, *37*, 785.
(67) Hay, P. J.; Wadt, W. R. *J. Chem. Phys.* **1985**, *82*, 270.
(68) Hay, P. J.; Wadt, W. R. *J. Chem. Phys.* **1985**, *82*, 299.
(69) Wadt, W. R.; Hay, P. J. *J. Chem. Phys.* **1985**, *82*, 284.
(70) Dunning, T. H., Jr. *J. Chem. Phys.* **1989**, *90*, 1007.
(71) Marten, B.; Kim, K.; Cortis, C.; Friesner, R. A.; Murphy, R. B.; Ringnalda, M. N.; Sitkoff, D.; Honig, B. *J. Phys. Chem.* **1996**, *100*, 11775.
(72) Friedrichs, M.; Zhou, R.; Edinger, S. R.; Friesner, R. A. *J. Phys. Chem. B* **1999**, *103*, 3057.
(73) Edinger, S. R.; Cortis, C.; Shenkin, P. S.; Friesner, R. A. *J. Phys. Chem. B* **1997**, *101*, 1190.
(74) Halgren, T. A.; Lipscomb, W. N. *Chem. Phys. Lett.* **1977**, *49*, 225.
(75) Peng, C. Y.; Schlegel, H. B. *Isr. J. Chem.* **1993**, *33*, 449.
(76) Fukui, K. *Acc. Chem. Res.* **1981**, *14*, 363.
(77) Gonzalez, C.; Schlegel, H. B. *J. Chem. Phys.* **1989**, *90*, 2154.
(78) Gonzalez, C.; Schlegel, H. B. *J. Phys. Chem.* **1990**, *94*, 5523.
(79) Murakami, M.; Itami, K.; Ito, Y. *Organometallics* **1999**, *18*, 1326.
(80) Osborn, J. A. *Chem. Commun.* **1968**, 1231.
(81) Bowden, F. L.; Giles, R. *Coord. Chem. Rev.* **1976**, *20*, 81.
(82) Shaw, B. L.; Stringer, A. J. *Inorg. Chim. Acta Rev.* **1973**, *7*, 1.